Supporting Information for "Experimental Monitoring of Nonlinear Wave Interactions Under Uniaxial Load"

Alison Malcolm [1], Lauren Hayes[1], Kamal Moravej[1], Andrey Melnikov[1],

Kristin Poduska[3], Stephen Butt[2]

[1]Department of Earth Sciences, Memorial University of Newfoundland

[2]Department of Engineering, Memorial University of Newfoundland

[2]Department of Physics and Physical Oceanography, Memorial University of Newfoundland

Contents of this file

1. Text S1 to S5

2. Figures S1 to S6

3. Tables S1 to S2

Introduction

This supporting information gives additional detail on the experimental setup not necessary for understanding the results, but necessary for duplicating the experiments. In addition, it gives more detail on the modeling of the strain induced by the pump and the cumulative strain observed by the probe.

Text S1: Measuring Velocity at Different Loads

It is important to calibrate transducers to have accurate travel time measurements by

————

December 2, 2021, 10:14am

measuring the travel time through different thicknesses of the same material and finding the intercept time. This intercept time measures the inherent delay from the transducer. For our transducers this number is 0.3 μs for S and 0.5 μs for P; we apply these corrections to the measured travel times before computing the associated velocities. To measure the velocities shown in Table 1 and Figure 5, we first pick the travel times. For the lowest applied load (1 MPa), this is done by picking the zero-crossing before the peak within a user-defined time window. Each pick is then manually checked to ensure that it chose the correct arrival. For higher loads, we measure the travel time change by cross-correlating the waveforms with those recorded at 1 MPa. When we extract the P-wave velocity from measurements of the S-wave PUMP, we are using what are sometimes referred to as parasitic P-waves, generated by S-wave transducers. In this case, the P-wave is much smaller than the S-wave and so to recover a reliable velocity change we window the data to include only the P-wave. This methodology along with estimates of the errors in P-wave velocities inferred from such parasitic waves is described by Yurikov et. al. (2019); they report errors of 5% compared with traditional methods of measuring P-wave velocities with P-wave transducers. We do not need to window when measuring the S-wave travel time because the S-wave is much stronger. For measurements on the probe signals, we record only about 2 periods of the signal and so there is no interference between different wavetypes. We measure the dimensions of the samples with calipers and use them to convert the travel times to velocities; these values are given in Table 1. We use the repeated measurements on the PUMP signals (for the two probes) to estimate the errors in our recovered velocities at less than 5%, in line with the errors from Yurikov et al. (2019) from using parasitic P-waves from S-transducers.

Text S2: Experimental details

All signals are generated with a standard (Agilent 33500B Series) function generator and recorded with a standard (KEYSIGHT InfiniiVision MSOX2014A) 8-bit oscilloscope. The pump signals are amplified with an (E & I 240L RF) power amplifier and all recorded signals are high-pass filtered with a (Krohn-Hite) adjustable digital filter with cut-off frequency of 600 kHz. Each recorded signal is an average of 4096 signals to reduce noise and sampled every 4 ns; example signals are shown in Figure 2. The signals are recorded at the lowest vertical range on the oscilloscope that does not result in clipping the recorded signal, this maximizes the accuracy of the recorded probe signal. This ranges from 1-200 mVp-p, except for when we record the PUMP alone (dotted lines in Figure 1) where the scale is 150 Vp-p.

We use Olympus transducers, specifically V-153 (S, 1 MHz, 1.3 cm diameter), V-103 (P, 1 MHz, 1.3 cm diameter) for the two probes and the V-1548 (S, 100 kHz, 2.5 cm diameter) for the PUMP. The driving frequencies of all transducers are chosen to give a signal recorded on the opposite face that most closely resembles our ideal waveform. For the pump this is a four-cycle sinusoid, and for the probe this is a one-cycle sinusoid. Example signals are shown in Figure 2.

All of our experiments were performed at room conditions, in an interior climate-controlled room. We wrapped the sample in plastic wrap to diminish the influence of humidity changes on the results. We would certainly expect to see changes in that environment over the course of the experiments, and the local humidity over the period of the experiment averaged 83% with significant excursions to a high of 100% and low of approximately 40%, with all days averaging between 75 and 95% and no consistent trends.

December 2, 2021, 10:14am

Experiments were completed on each sample and probe before moving to the next to minimize the effect of variations in room conditions on the results. Khajehpour Tadavani et. al. (2020) find that humidity changes impact the results, but that these impacts have an exponential time constant on the order of days to weeks for these samples, in other words these changes happen slowly compared to our experimental time.

Text S3: Measuring the strain This strain is measured using a laser-doppler vibrometer and averaging the amplitude (measured from the peak of the Hilbert transform of the signal) of the recorded particle velocity signals at several locations on the sample. We then divide the recorded particle velocity by the phase velocity of the recorded wave. This gives an estimate of the strain assuming that we are exciting plane waves. Because this assumption is not strictly true, we are confident only that this gives us the order-of-magnitude of the strain and that it gives us a good measure of the relative magnitude of the two strains. This is the same protocol as used by Gallot et al. (2015), repeated on this sample in our laboratory. It is explained in more detail by Khajehpour Tadavani et al. (2020).

Text S4: Computing the travel time delays We compute the travel time delays plotted on the y-axis in Figure 6 by fitting a sinc function to the five points nearest the peak of the cross-correlation of the two signals. This follows the suggestion of e.g. Catheline et al. (1999), replacing the parabola with a sinc function because in fitting the peak we are essentially assuming that we have undersampled our signals, for which a sinc interpolation is the optimal solution (Ali Gholami, personal communication, 2018). Our numerical experiments using one-cycle sine waveforms shifted by a known amount indicate that we can estimate a travel time delay with two digits of accuracy down to

approximately 1/100 of our sampling interval (i.e. the error in our travel time estimate is 0.04 ns).

Text S5: Modeling Strain

The goal of this section is to explain what our measurements are sensitive to. More specifically, we aim to demonstrate which parts of the pump waveform cause the perturbations we observe when we measure delays in the travel time of the probe wave. To this end, we model both waveforms through a sample that is meant to be close to both of the samples used in the experiment. The parameters of the model rock are given in Table S1. The code we use is a standard staggered-grid finite-difference algorithm (Virieux, 1986; Graves, 1996). The numerical parameters are given in table S2. This code computes the particle velocity and stresses; we compute the strain from the stresses using a linear Hooke's law. We use reflecting boundaries on all sides. Our goal is to estimate the cumulative strain, caused by the pump, that is sensed by the probe wave during our experiments. To this end, we show the results of three experiments. The first simulation is to verify the accuracy of our transducer model. This simulation is compared with a separate set of experimental data to verify that our modeled transducer does indeed agree with our experimental equipment, and uses a grid and geometry, described below, appropriate to that experiment. The second dataset we compute models the probe, which uses a fine mesh and a scaled-down model because of the higher frequency of the probe signal. This simulation is used to verify that our assumptions about where this signal is in space and time are accurate. The third experiment models the propagation of the pump. We first use these simulated data to compare with our experimentally recorded pump signal and evaluate the accuracy of the numerical model. We then use this simulation to estimate

December 2, 2021, 10:14am

the observed strain distribution in the sample for a variety of pump/probe delays from which we estimate the cumulative strain the probe wave will see as it travels across the sample. This simulation is done on a coarser grid and thus we are able to simulate the wave propagation throughout the larger sample.

We begin by checking the transducer model. We model the source transducer as a set of 492 point-forces distributed over a circular region on one face of the model. We do not weight the sources in any way, so all contribute equally to the generated waves. To verify that this is sufficiently accurate, we compare our modeled transducer radiation pattern with a recorded radiation pattern. The relevant numerical parameters are given in table S2. The experimental dataset that we compare to is measured in a homogeneous plexiglas sample. The experimental geometry is shown in Figure S1. We send a single cycle of a 200 kHz sine function to the source P-wave transducer (the same make and model as that used as the P-wave probe source in our other experiments) in the positive y-direction, and a laser doppler-interferometer measures the same y-component of the particle velocity on the opposite side of the sample. The experimental data are collected on a line and then corrected for geometrical spreading to recover the radiation pattern. For the numerical data, we excite a y-direction force on a simulated transducer with radius of 5 mm to match our transducer's active radius. We then record the mdoel data on an array of detectors on a circle of radius 2 cm centered on the transducer center to avoid the need for a geometrical spreading correction. We see in Figure S1 that the agreement between the experimental and modeled data are excellent. We thus conclude that our transducer model is adequate for the probe transducer when it is driven at 200 kHz. We now must ask if this translates to our probe signal, which is at a higher frequency. Although the only

way to know for certain is to do the experiment, the transducer is designed to respond linearly over a relatively wide frequency range, and so we do not anticipate significant deviations. For the PUMP signal, the argument is similar. It is a different transducer and different frequency range, but manufactured by the same company using the same technology. We thus expect that this model is sufficient for our purposes. In addition, this is the same modeling strategy and code used by Gallot et al. (2015) where they were able to obtain excellent agreement between the signal recorded with the laser on the surface (though they did not look at this agreement as a function of position).

Next, we look at the propagation of the probe. This is expected to be quite straight-forward as it is a small wave, likely in the linear regime, and it propagates directly from the source transducer to an identical receiver transducer on the opposite face. Because of the high-frequency of this signal, this simulation requires a small spatial sampling inter-val, which can be challenging numerically as it takes a great deal of memory to run the simulation. To mitigate these extreme memory requirements, we reduce the size of the model to be only $5 \times 15 \times 5$ cm in x, y, z, as shown in Figure S2. This will not result in an accurate waveform for the parts of the wave that arrive after the direct arrival as the scattering from the boundaries is significantly enhanced in this smaller simulation, but this scattering will not affect the direct arrival that we are interested in. Snapshots of the wavefield at several times are shown in Figure S2. On top of these snapshots, we plot an ellipse with major axis the size of the transducer and minor axis one wavelength. We also show, with two horizontal lines, the extent of the transducer. We assume that the transducer will measure only those signals that arrive between these two white lines. In what follows, we will use the pump strain within this ellipse to calculate the cumulative

strain that the probe sees as it travels across the sample. We see that the ellipse tracks

this first-arriving wave across the sample and includes the dominant part of the signal.

Little difference is anticipated if we change the details of the shape or size of this elliptical

domain. We show the ϵ_{yy} component of the strain because this is the component that we

dominantly excite and observe for a P-wave travelling in the y-direction. Although the

shape of the strain changes if we look at different components, the extent and travel time

does not, so we do not expect significant changes to these ellipsoidal regions if we were to

look at different strain components.

Now that we have verified that we are able to simulate our transducer response and that

the simulated probe wave travels directly across the sample in a way that is easily tracked,

we now model the pump signal. Figure S3 shows the model setup and the modeled pump

signal recorded on virtual transducers located within the sample. The displayed signal is

the average of all of the signals recorded within the area of the transducer, which is set

to correspond with the physical transducer located on the bottom of the sample in the

physical experiment. Varying the number of recording locations within the transducer or

even looking at the response at a single detector has only a minor influence on the results.

We model the data at 100 kHz rather than the 90 kHz at which we drove the physical

transducer because the spectrum of the data (shown in Figure S3 for a recording from the

center of the sample in (x, z) and the bottom in x, specifically (x, y, z)=(12.6, 7.5, 2.5) cm)

has a spectrum centered closer to 100 kHz than to 90 kHz. We show the modeled signal

at several depths because our model is linearly elastic whereas our sample exhibits both

nonlinearities and is clearly visco-elastic. In addition, the numerical boundary conditions

are not perfect and we model the edges as though they are perfectly flat surfaces, which

they are not. These effects combine to make the boundary reflections significantly stronger in the model than they are in the data. We conclude this by comparing the recorded data with the modeled data at both $x = 12.5$ cm and $x = 5.5$ cm. At $x = 12.5$ cm we would expect the experimental and modeled data to agree, but they clearly do not. The waves arrive at approximately the same time (there is no shift in the experimental data on this sub-plot), but do not have the same waveform. By contrast, when looking at the data at $x = 5.5$ cm the times do not agree as expected (the modeled data are shifted), but the waveform shapes are nearly identical. In the data at $x = 5.5$ cm, there is a clear boundary reflection arriving after the direct wave. These two waves would be expected to be on top of one another when the data are recorded directly on the boundary, which changes the shape of the modeled waveform. Based on this comparison, we conclude that the modeled data are giving a more complicated picture of the waveforms than are likely present in the physical experiment, but this picture still captures the majority of the phenomena of interest particularly away from the edges of the sample.

Having discussed the validity of the model, we now use it to track the cumulative strain. This follows a procedure identical to that in (Gallot et al., 2015), which we describe briefly here. We model the strain caused by the pump, snapshots of the ϵ_{xy} component are shown in Figure S4, with the locations of the P- and S-probes overlain for various transmission delays. Using these snapshots, we then compute the cumulative strain for the AB-component of strain, ϵ_{AB}

$$e_{AB}^{cum}(\tau) = \frac{1}{|S|} \int_S \int_0^{T_{max}} \chi(x, t - \tau)\epsilon_{AB}(x, t)dxdt \tag{S.1}$$

where S is the path along which the probe travels, $|S|$ is its length, and χ is an indicator function that is equal to one in the vicinity of the probe wave and zero elsewhere. We

compute this cumulative strain for a range of phase shifts, τ, covering the range that we use in the experiments and more, and use strains up to a time of $T_{max} = 200$ μs, which is approximately the time it takes the pump wave to travel across the sample and then back to the source. Our procedure is to take the computed $\epsilon_{AB}(x, t)$ from the pump propagation and then multiply it by $\chi(x, t - \tau)$, where χ is supported (=1) on the ellipse described above and shown in Figure S4, and zero elsewhere. The remaining strain is then added to the strain from the previous (x, τ)-pair until either the probe reaches the opposite side of the sample or we run out of times for the pump. We repeat this process for different transmission delays and show the results of the cumulative strain in Figure S5. Because the path is a straight line, $|S|$ is constant and the same for all measurements.

Figure S5 shows the cumulative strain, computed using e_{yy}, for the P-wave probe and Figure S6 shows the cumulative strain, computed using e_{yz} for the S-wave probe. The first key point to note is that the cumulative strain is oscillatory, with the period of the pump, and with a shape that echoes the general shape of the pump, with some modifications caused by both boundary effects and from the integration. In the first panel of both figures, we test whether or not the waves interact primarily in the central region of the sample. This serves to test both whether or not inaccuracies in the model are strongly influencing the estimated accumulated strain and to test whether the central region of the strain field is more important to the interactions than the edge regions. For this test, we progressively remove more of the edges of the sample from the integration region. Specifically, before computing the integration we remove the contribution from the edges by setting $\epsilon_{AB}(x, Y_{max} - Y_{perc/2} < y < Y_{max}, z) = 0$ and $\epsilon_{AB}(x, Y_{min} < y < Y_{min} + Y_{perc}/2, z) = 0$, where Y_{max}/Y_{min} are the maximum/minimum y-value and Y_{perc}

is the percentage of the data set to zero and e_{AB} is the AB component of the strain tensor. From this plot, we see that the magnitude of the cumulative strain changes when we exclude parts of the sample, but the shape (as a function of time) does not. As a second test, we look at how the cumulative strain changes if we estimate it with different components of the modelled strain. This test is shown in (b) of Figure S5 and Figure S6. In this case, we see that the details of the shape change, but the strong component at the frequency of the pump remains whichever component of the strain we use. This gives us confidence that the cumulative strain is indeed an oscillatory function at the frequency of the pump. This helps to explain the signals that we observe; we see oscillations at the frequency of this cumulative strain with the sort of softening that is common in nonlinear experimental observations.

:

Table S1. Physical parameters for the numerical model.

Physical Parameters	
V_P	3.1 mm/μs
V_S	2.1 mm/μs
ρ	2.4 kg/m^3

	xmax	ymax	zmax	dx=dy=dz	dt	f	nperiods	srad	sdir	fdir
radiation pattern										
	50 mm	155 mm	52 mm	0.75 mm	50 ns	200 kHz	1	5 mm	x	x
probe										
	50 mm	155 mm	52 mm	0.1 mm	10 ns	1 MHz	1	5 mm	x	x
PUMP										
	126 mm	155 mm	52 mm	1 mm	100 ns	100 kHz	4	12.5 mm	z	x

Table S2. Numerical parameters used in the experiments. nperiods is the number of periods in the input source waveform (all use a sinusoid), sdir indicates the direction the source wave travels and fdir the direction of the applied force.
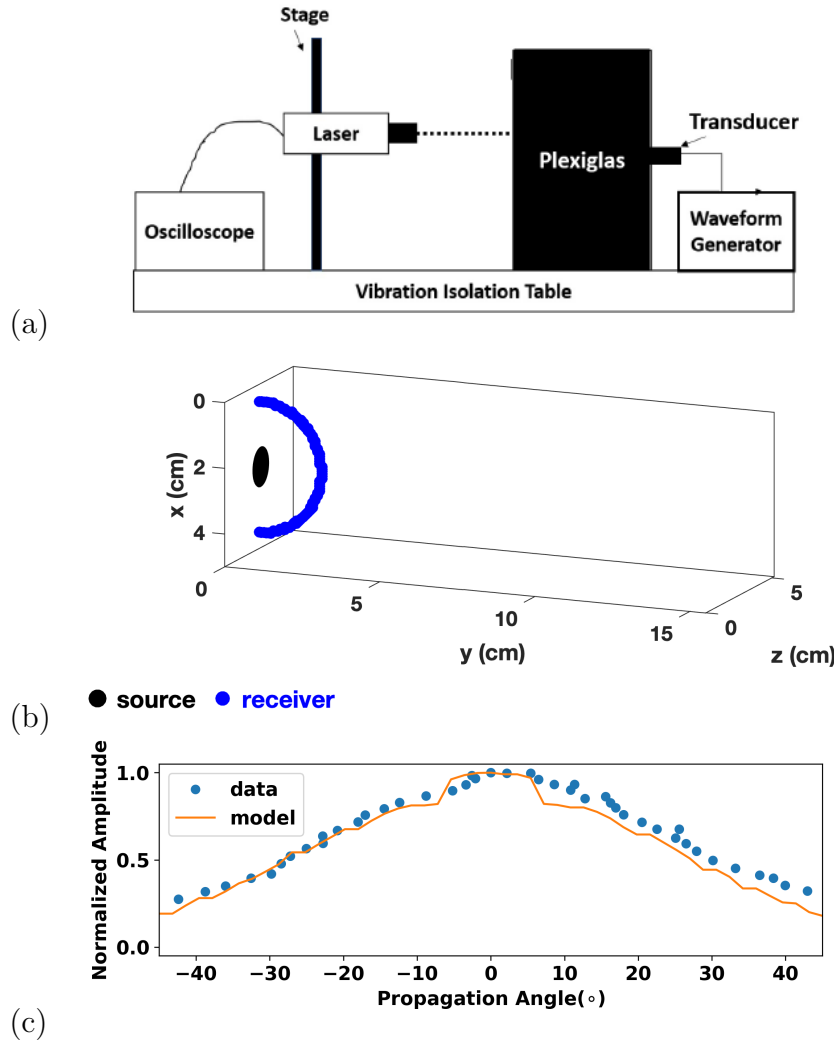
December 2, 2021, 10:14am

(a)

(b)

(c)

Figure S1. (a) Experimental configuration for measurement of the radiation pattern of the transducer. (b) Numerical experimental configuration for the measurement of the radiation pattern. (c) Comparison of the measured and modeled radiation patterns.
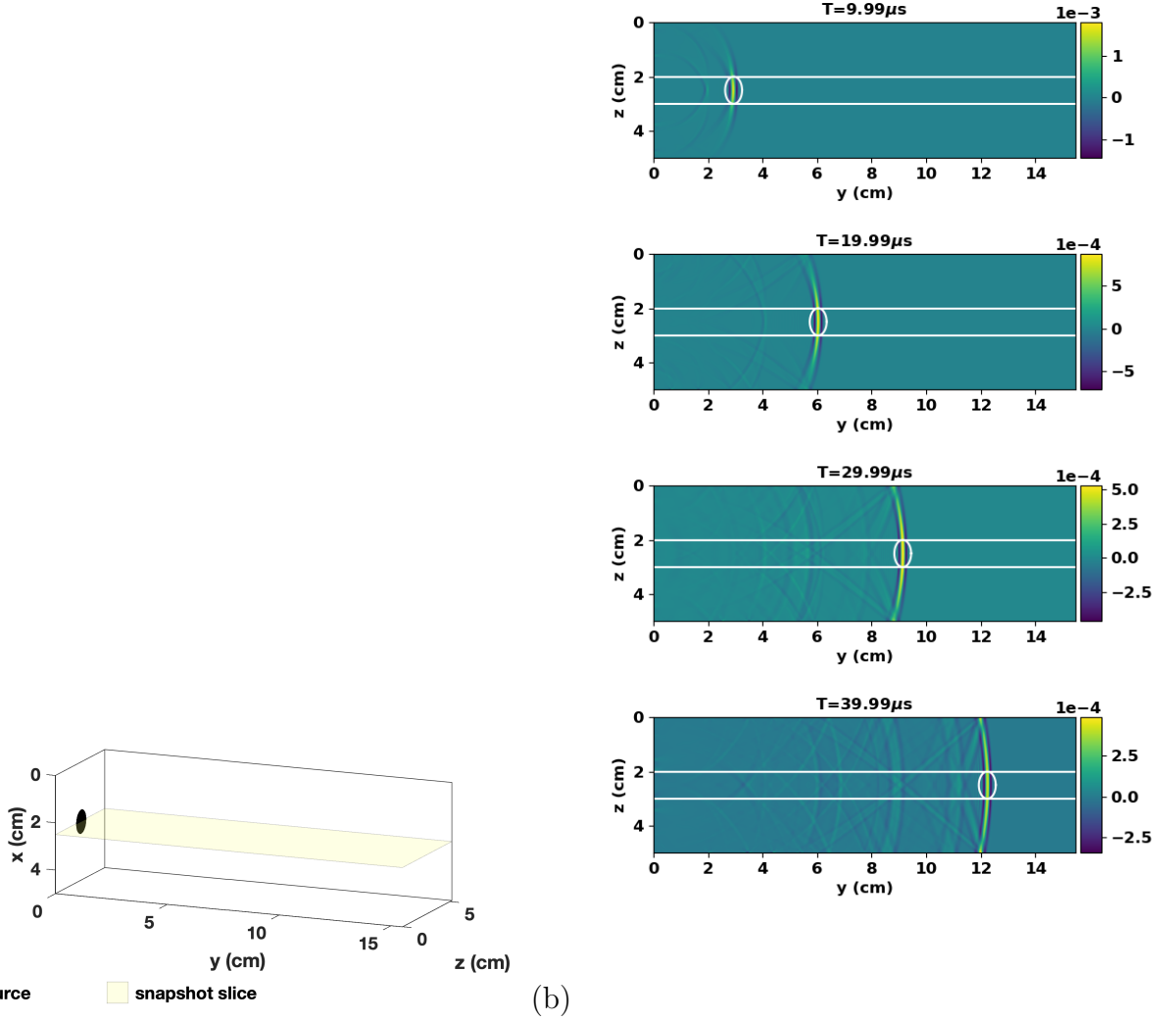
(a) ● source   ▢ snapshot slice   (b)

Figure S2. (a) Numerical Experimental Geometry for probe model. The yellow region highlights the location of the snapshots plotted below. (b) ϵ_{yy} for the probe signal at different times. The white lines show the boundaries of the transducer. The white ellipse shows the region included in the cumulative strain calculation. This shows that the probe signal is easily predicted.
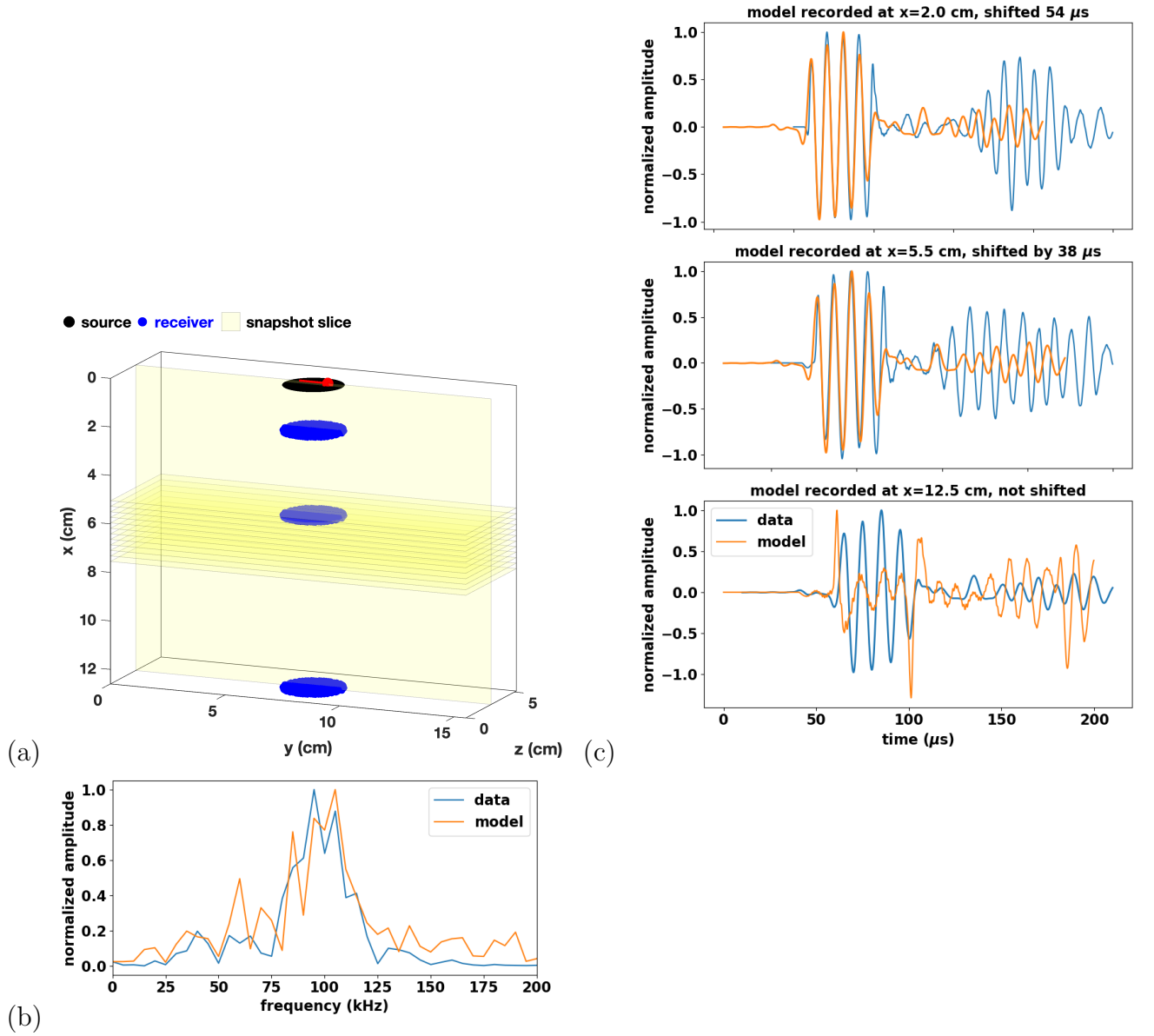
(a)

(b)

(c)

Figure S3. (a) Experimental setup for the PUMP model. The yellow regions show where snapshots are recorded; data from the vertical slice and the central horizontal slice are shown in Figure S4, and data from all of the horizontal slices are used in the computations shown in Figure S5. (b) Spectrum of the data (recorded at $(x, y, z) = (12.6, 7.5, 0.0)$ cm). (c) Comparison of the modeled and recorded signals at the top, middle, and bottom of the sample. The location of the receivers are shown as blue dots in the top panel. All data are normalized and we have shifted the experimental data to align with the first peak of the modeled data; the shifts are given in the individual plot titles.
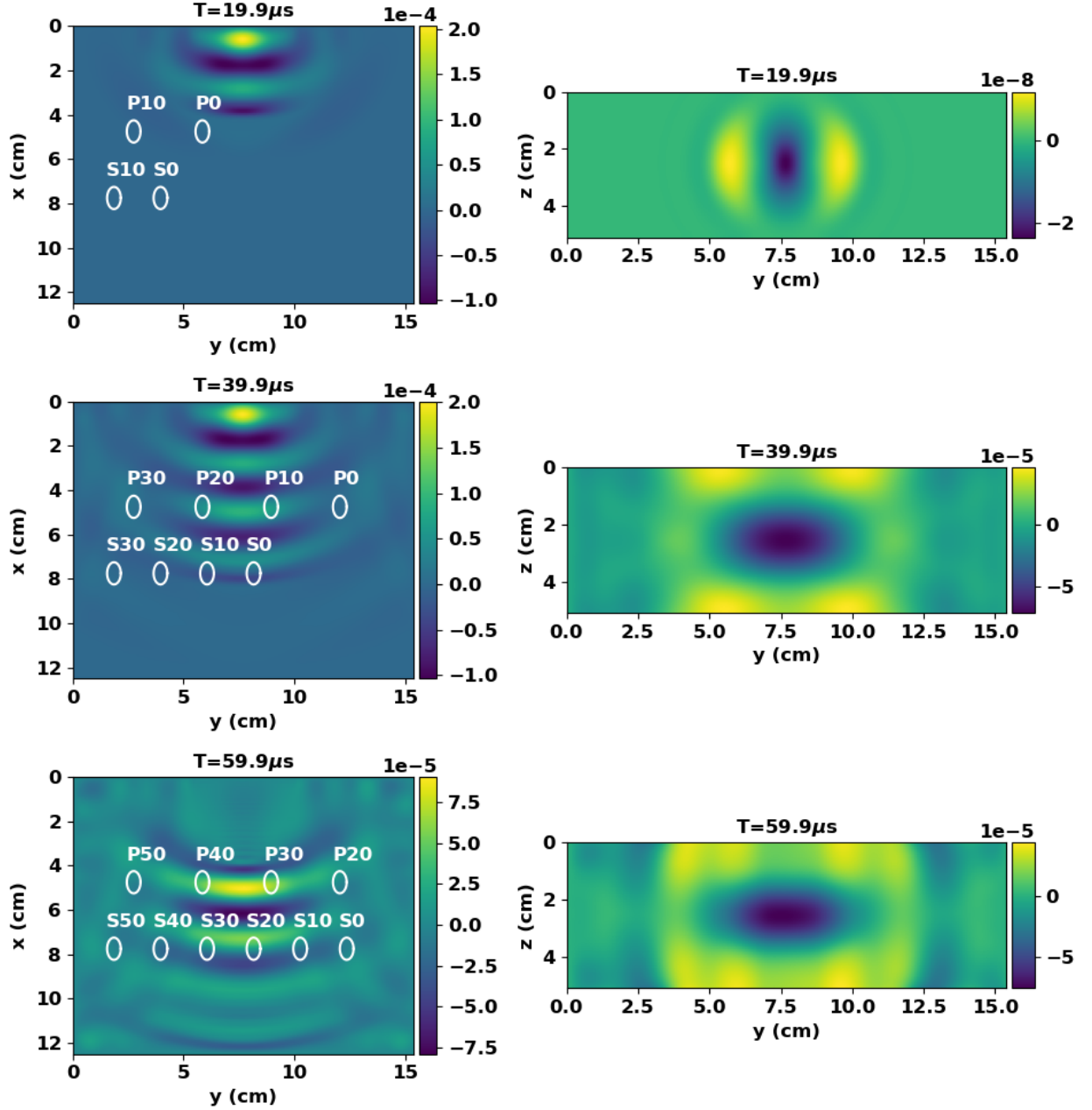
:

Figure S4. Snapshots of the PUMP wavefield (the e_{yx}-component as a function of time (plot title gives the time of the snapshot). The white ellipses outline the probe location for various delays (text above ellipses, in μs). The left column shows the vertical snapshot and the right column the central horizontal snapshots.
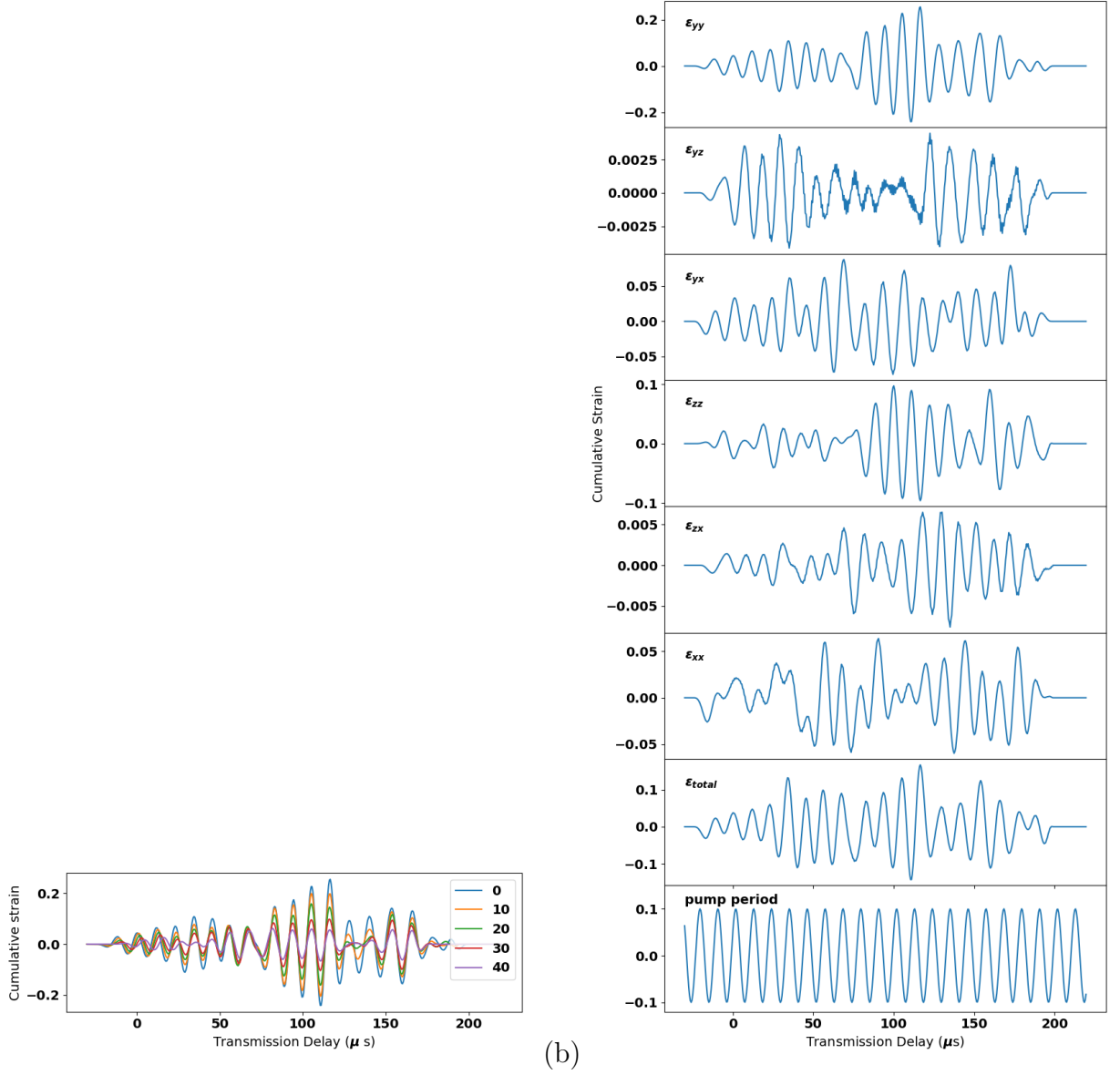
December 2, 2021, 10:14am

Figure S5. Cumulative strain for the P-probe. (a)Cumulative strain calculated with e_{yy}, as a function of the percentage Y_{perc}, of the model left out of the calculation (removed symmetrically from both sides); the legend number gives the value of Y_{perc} with units of %. (b) Cumulative strain computed using different input strain components. The bottom plot shows a sinusoid at the frequency of the pump with arbitrary phase. Note that each plot in (b) has its own y-axis values.
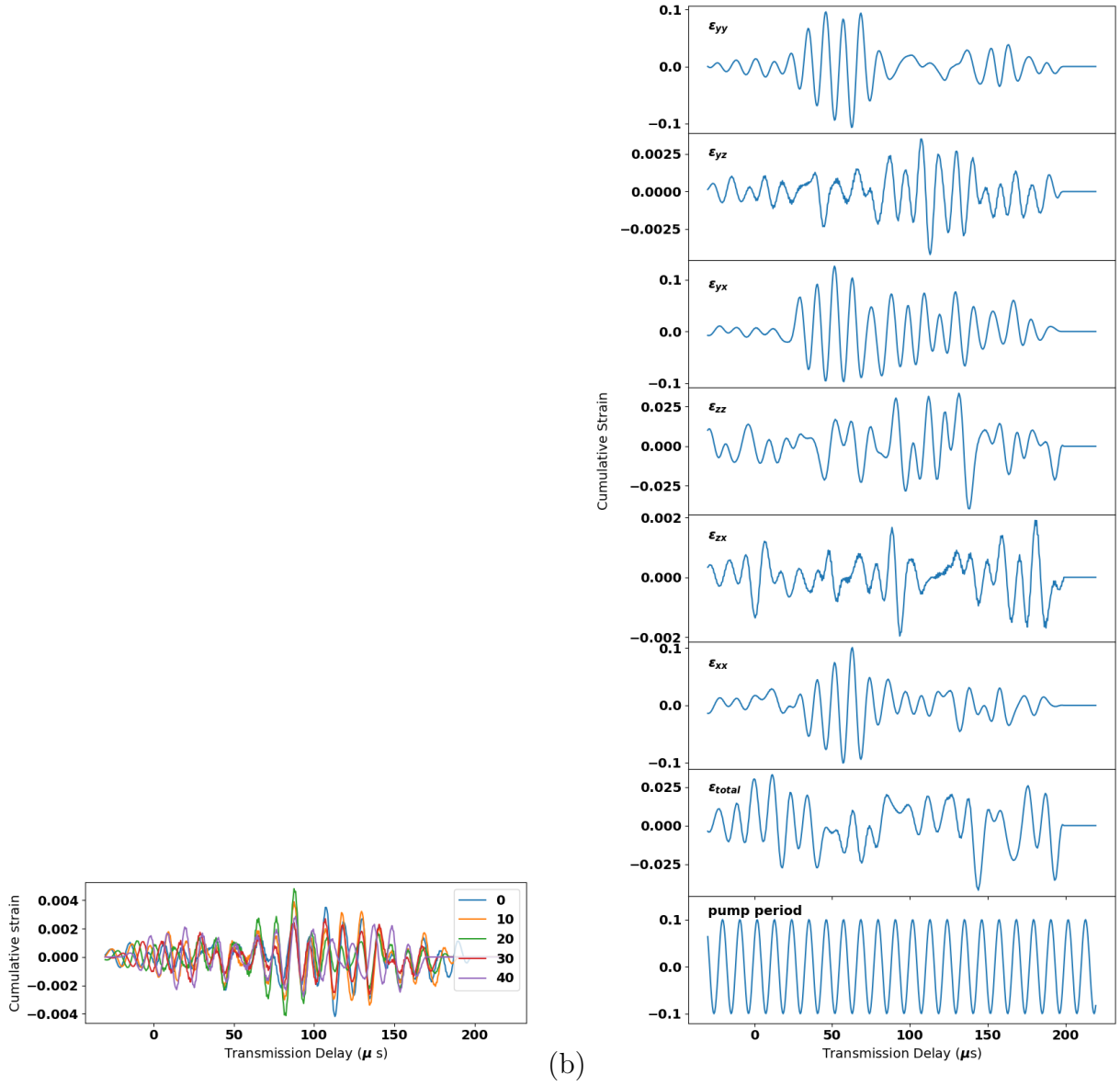
Figure S6. Cumulative strain for the S-probe. (a) Cumulative strain calculated with e_{xy} as a function of the percentage of the model left out of the calculation (removed symmetrically from both sides). (b) Cumulative strain computed using different input strains components. The bottom plot shows a sinusoid at the frequency of the pump with arbitrary phase. Note that each plot in (b) has its own y-axis values.